Visualization and Classification of Amyloid β Supramolecular Assemblies†

Hisashi Yagi,‡ Tadato Ban,§ Kenichi Morigaki,§ Hironobu Naiki,|| and Yuji Goto*,‡

Institute for Protein Research, Osaka University, and CREST, Japan Science and Technology Agency, Yamadaoka 3-2, Suita, Osaka 565-0871, Japan, National Institute of Advanced Industrial Science and Technology, Midorigaoka 1-8-31, Ikeda, Osaka 563-8577, Japan, and Department of Pathological Sciences, Faculty of Medical Sciences, University of Fukui, and CREST, Japan Science and Technology Agency, Eiheiji, Fukui 910-1193, Japan

Received September 10, 2007; Revised Manuscript Received October 23, 2007

ABSTRACT: Deposition of amyloid β (Aβ) fibrils has been suggested to play a central role in Alzheimer's disease. In clarifying the mechanism by which fibrils form and moreover in developing new treatments for amyloidosis, direct observation is important. Focusing on the interactions with surfaces at the early stages, we studied the spontaneous formation of Aβ(1−40) fibrils on quartz slides, monitored by total internal reflection fluorescence microscopy combined with thioflavin T, an amyloid-specific fluorescence dye. Self-assembly of Aβ(1−40), accelerated by a low concentration of sodium dodecyl sulfate, produced various remarkable amyloid assemblies. Densely packed spherulitic structures with radial fibril growth were typically observed. When the packing of fibrils was coarse, extremely long fibrils often protruded from the spherulitic cores. In other cases, a large number of wormlike fibrils were formed. Transmission electron microscopy and atomic force microscopy revealed relatively short and straight fibrillar blocks associated laterally without tight interaction, leading to random-walk-like fibril growth. These results suggest that, during spontaneous fibrillation, the nucleation occurring in contact with surfaces is easily affected by environmental factors, creating various types of nuclei, and hence variations in amyloid morphology. A taxonomy of amyloid supramolecular assemblies will be useful in clarifying the structure−function relationship of amyloid fibrils.

The deposition of amyloid fibrils in extra- and intracellular spaces is responsible for various neurodegenerative disorders, e.g., Alzheimer's (AD),[1] Parkinson's (PD), prion, and polyglutamine diseases and dialysis-related amyloidosis (*1*−*3*), in which the formation of amyloid fibrils has common features of nucleation, extension, and seeding (*4*−*6*). Recent studies have shown that, although many proteins and peptides form amyloid or amyloid-like fibrils (*7*−*10*), the main chain backbone of amyloid fibrils is arranged in a common cross-β structure oriented perpendicular to the fibril axis independent of protein or peptide species (*8*, *11*). In contrast, the morphology of amyloid deposits can vary dramatically even for one protein depending on the tissue and disease conditions (*12*). Exhibition of both polymorphism, the ability of one polypeptide to form aggregates of different morphologies, and isomorphism, the ability of different polypeptides to grow into a common fibrillar amyloid morphology, has been proposed to be an important feature of amyloid fibrils, more resembling plastic materials generated from synsthetic polymers than globular proteins (*13*, *14*). These suggest that the variation of amyloid supramolecular assemblies is a key to understanding the role of fibrils in diseases, including neurotoxicity and transmission of amyloidoses (*15*−*19*).

Most morphological investigations of amyloid fibrils have been performed with electron microscopy (EM) (*20*−*22*). Recently, atomic force microscopy (AFM) has become a major method, making direct observations of fibril growth possible (*17*, *23*, *24*). The direct observation of fibril growth provides essential information about the mechanism of fibrillation, which cannot be obtained with conventional spectroscopic methods. More recently, we developed a new approach to monitoring fibril growth in real time at the single fibril level, in which total internal reflection fluorescence microscopy (TIRFM) was combined with the use of thioflavin T (ThT) (*24*−*27*).

Amyloid β (Aβ) peptide has been the most widely studied of the various amyloidogenic proteins and peptides (*28*−*30*). Aβ is an ∼43-amino acid product of the amyloid precursor protein cleaved by β- and γ-secretases and deposited in extracellular spaces as senile amyloid plaques, a pathological hallmark of AD. Additionally, deposition on vascular basement membranes has been documented (*12*). In vivo, for several proteins, including Aβ, interaction with membranes (i.e., basement or plasma membranes) affected their fibrillation (*31*, *32*), often producing radial and spherical aggregates of fibrils governed by fibril−fibril or fibril−membrane interaction (*33*). Because of limitations to the

† This work was supported by the Takeda Science Foundation, by Grants-in-Aid from the Japanese Ministry of Education, Culture, Sports, Science and Technology on Priority Areas (40153770), and by Japan Society for Promotion of Science (JSPS) Research Fellowships for Young Scientists to T.B.

* To whom correspondence should be addressed. E-mail: ygoto@protein.osaka-u.ac.jp.

‡ Osaka University.

§ National Institute of Advanced Industrial Science and Technology.

|| University of Fukui.

[1] Abbreviations: AD, Alzheimer's disease; PD, Parkinson's disease; β2m, β_2-microglobulin; Aβ, amyloid β; TIRFM, total internal reflection fluorescence microscopy; EM, electron microscopy; TEM, transmission electron microscopy; AFM, atomic force microscopy; ThT, thioflavin T; SDS, sodium dodecyl sulfate; CMC, critical micelle concentration.

10.1021/bi701842n CCC: $37.00
Published on Web 11/29/2007

structural investigation of amyloid fibrils in vivo, direct and real-time observations in vitro of fibril growth in a membranelike environment are needed.

Previously, we reported that the surface properties of quartz slide glasses affect the formation of Aβ(1−40) fibrils, suggesting the underlying mechanism by which senile plaques form (*27*). However, because those experiments used seed-dependent growth, the mechanism of fibrillation without seeds remains obscure. In this study, we examined the spontaneous formation of Aβ(1−40) fibrils on the quartz surface, focusing on the nucleation process. Growth and fibril morphology depend on nuclei and thus influence cytotoxicity (*34*). In vivo, many amyloidogenic proteins and peptides interact with the basement membrane surface (*32*). Therefore, pathways leading to fibrils are considered to depend critically on the surface properties. On the basis of the observed dramatic diversity and underlying structural basis, we propose a taxonomy of amyloid supramolecular assemblies.

MATERIALS AND METHODS

Fibril Formation and Thioflavin T Assay. Aβ(1−40) and Aβ(1−42) peptides were purchased from the Peptide Institute (Osaka, Japan). The peptides were dissolved in an ammonia solution [0.5% for Aβ(1−40)] to a concentration of 500 μM and immediately stored at −85 °C. Aβ(1−40) at 50 μM was incubated in 50 mM sodium phosphate buffer (pH 7.5) containing various concentrations of NaCl (0.1−1.0 M) and sodium dodecyl sulfate (SDS) (0.2−0.5 mM) without agitation, and the formation of fibrils was monitored via a ThT binding assay (*35*) using a Hitachi F-4500 fluorescence spectrophotometer. Aliquots were mixed with 5 μM ThT in glycine-NaOH buffer (pH 8.5), and fluorescence intensity was monitored at 490 nm with excitation at 445 nm.

Direct Observation of Amyloid Fibrils. The TIRFM system used to observe individual amyloid fibrils was developed on the basis of an inverted microscope (IX70, Olympus, Tokyo, Japan) as described previously (*25*, *26*, *36*). The ThT molecule was excited at 442 nm by a helium−cadmium laser (IK5552R-F, Kimmon, Tokyo, Japan). The fluorescence image was filtered with a band-pass filter (D490/30, Omega Optical, Brattleboro, VT) and visualized using a digital steel camera (DP70, Olympus). The peptides were dissolved in an ammonia solution [0.5% for Aβ(1−40), 0.05% for Aβ-(1−42)] to a concentration of 500 μM and immediately stored at −85 °C. Aβ(1−40) (50 μM) was incubated in 50 mM sodium phosphate buffer (pH 7.5) containing various concentrations of NaCl (0.1−1.0 M) and SDS (0.2−0.5 mM), and Aβ(1−42) (50 μM) was incubated in 50 mM sodium phosphate buffer (pH 7.5) containing 0.5 M NaCl and 0.5 mM SDS, or 0.1 M NaCl without SDS. ThT (100 μM) was added at a final concentration of 5 μM. An aliquot (14 μL) of sample solution was immediately deposited on each microscopic slide and incubated at 37 °C for 1−2 days, and an image of the fibrils was obtained with TIRFM. Parallel flat quartz substrates were obtained from Hikari Kobo (Tokyo, Japan) and were used without modification of surfaces.

For the seed-dependent growth, seeds of Aβ(1−40) were prepared by the fragmentation of amyloid fibrils for 5 min with a TAITEC (Saitama, Japan) VP-30S sonicator equipped with a microtip. The seeds were added at a final concentration of 0.5 μg/mL to 50 μM monomeric Aβ(1−40) in polymerization buffer [50 mM sodium phosphate (pH 7.5) containing 0.5 M NaCl and 0.5 mM SDS]. The ThT solution was then added at a final concentration of 5 μM. Sample mixtures were deposited on the quartz slide surface, and fibrils were observed under TIRFM at 37 °C.

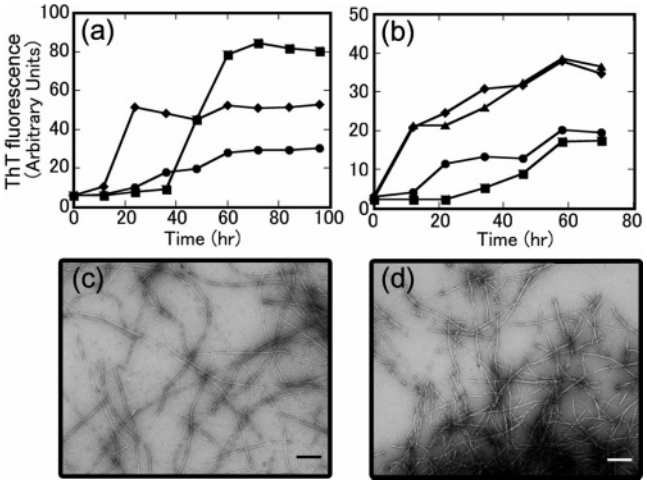

FIGURE 1: Formation of Aβ(1−40) fibrils under various conditions at pH 7.5, monitored by a ThT binding assay. (a) Effects of NaCl at concentrations of 0.1 (■), 0.5 (●), and 1.0 M (◆). (b) Effects of (■) 0.1 M NaCl and 0.25 mM SDS, (●) 0.1 M NaCl and 0.5 mM SDS, (▲) 0.5 M NaCl and 0.25 mM SDS, and (◆) 0.5 M NaCl and 0.5 mM SDS. Electron micrographs of Aβ(1−40) fibrils showed those at 0.1 M NaCl (c) and at 0.5 mM SDS and 0.5 M NaCl (d). The scale bar represents 200 nm.

Transmission Electron Microscopy. The rigid-straight or wormlike fibrils were examined by transmission electron microscopy (TEM). After confirmation of the formation of fibrils via TIRFM, the cover slip was carefully removed from the quartz substrate. An aliquot (5 μL) of distilled water was deposited on the substrate, and then carbon-coated copper grids (400 mesh) (Nissin EM, Tokyo, Japan) were put on the substrate for 2 min to transfer the fibrils. Next, the samples were stained with a 2% (w/v) uranyl acetate solution. TEM images were acquired using a transmission electron microscope (100CX, JEOL, Tokyo, Japan) at 80 kV with a magnification of 29000×.

Atomic Force Microscopy. AFM images were acquired using a Digital Instruments Nanoscope IIIa scanning microscope at 25 °C (Veeco, Tokyo, Japan). Measurements were performed using an air tapping mode. After confirmation of the formation of wormlike fibrils via TIRFM, the cover slip was carefully removed and the quartz substrate was cut by diamond pencil to adjust the AFM sample stage. The quartz surface was scanned directly to examine the fibril morphology.

RESULTS

Self-Assembly of Aβ(1−40) into Amyloid Fibrils in Test Tubes. Previously, we examined the seed-dependent growth of Aβ(1−40) fibrils under neutral-pH conditions [50 mM sodium phosphate (pH 7.5) containing 0.1 M NaCl] (*26*, *27*), where the spontaneous formation of fibrils required ∼3 days (Figure 1a). A long incubation (>3 days) on the slide glass tended to dry the samples, making TIRFM experiments difficult. In fact, few fibrils were observed by TIRFM (data

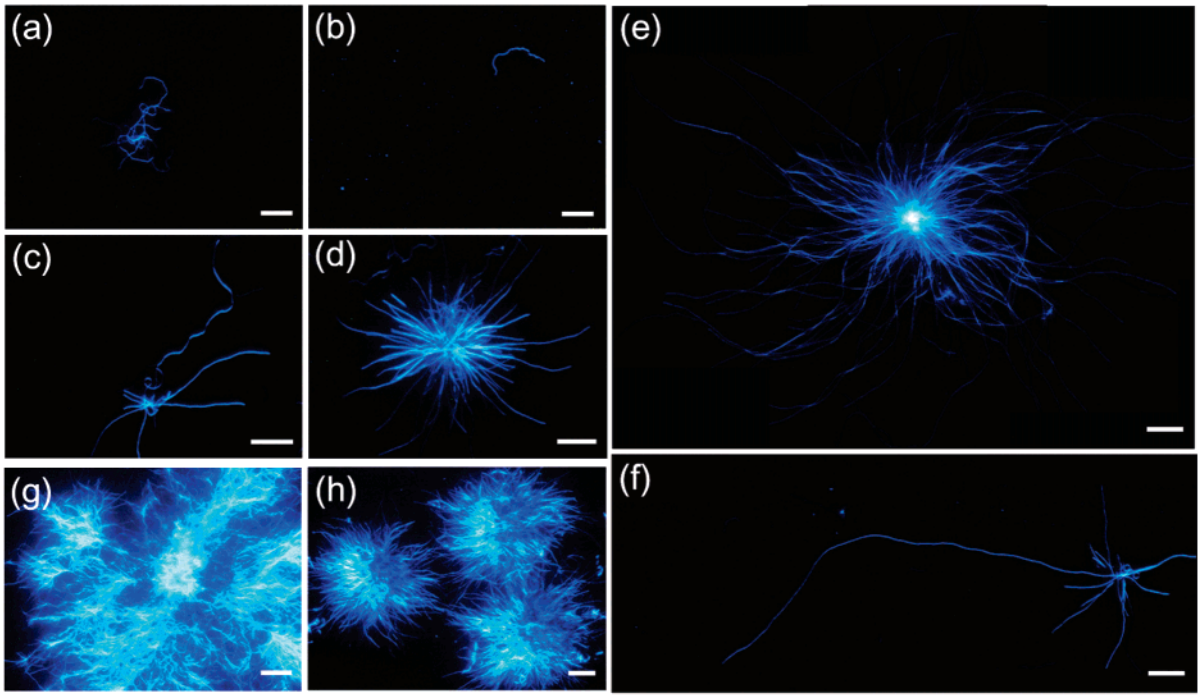

FIGURE 2: Unique morphology of Aβ(1−40) fibrils at various concentrations of NaCl and SDS on the quartz. (a) A few fibrils were observed at 0.5 mM SDS in 0.25 M NaCl after incubation for 26 h. (b) A low concentration of SDS (0.25 mM) in 0.5 M NaCl did not produce many fibrils after incubation for 13 h. (c−f) Unique morphology observed at 0.3 mM SDS and 0.5 M NaCl: twisted fibrils (c), spherulitic fibrils (d), long fibrils protruding from huge spherulitic assemblies (e), and a tremendously long fibril (f). (g and h) Densely packed spherulitic structures formed in 0.5 mM SDS and 1.0 M NaCl. The scale bar represents 10 μm.

not shown). Thus, we attempted to accelerate the spontaneous fibril growth.

First, we increased the NaCl concentration, which is known to enhance the rate of aggregation of monomer Aβ-(1−40) (*37*). The formation of fibrils of Aβ(1−40), monitored by the ThT binding assay (*35*), was promoted at 1.0 M NaCl (Figure 1a): the lag time was shortened from 36 to 12 h. However, these samples also revealed few amyloid fibrils by TIRFM (data not shown). Second, because SDS at a level near the critical micelle concentration (CMC) enhanced the nucleation of β_2-microglobulin (β2m) (*38*), we added SDS to the conditions described above (*23*). The addition of 0.5 mM SDS indeed promoted the formation of Aβ(1−40) fibrils without lag time (Figure 1b). Moreover, we observed a large number of Aβ(1−40) fibrils by TIRFM (see below). It is known that GM1 ganglioside bound to Aβ induces Aβ assembly in vivo (*39*). We consider that, in a similar way, SDS mimics the membrane environment, efficiently triggering the spontaneous formation of Aβ(1−40) fibrils. On the other hand, Cruz et al. (*40*) suggested that, in the presence of a high concentration of salt ions, salt bridges play a more prominent role in the stabilization of the loop (Val 24−Lys 28) of Aβ(1−40) fibrils, thus forming nuclei rapidly. Therefore, we used the conditions that included 0.5 mM SDS for spontaneous fibrillation of Aβ(1−40).

We then analyzed the morphology of amyloid fibrils formed with or without SDS by TEM (Figure 1c,d). Without SDS at 0.1 M NaCl, long straight fibrils with a diameter of 12 ± 2 nm were observed. On the other hand, with 0.5 mM SDS at 0.5 M NaCl, short straight fibrils with a diameter of 13 ± 2 nm dominated. These results suggest that, although SDS increases the number of initiation sites (i.e., nuclei) and accelerates growth, the morphology of amyloid fibrils is basically independent of SDS.

Formation of Aβ(1−40) Fibrils on the Quartz Surface. We then examined the fibrillation of Aβ(1−40) on the quartz surface, which was monitored by TIRFM. We first confirmed the effects of various concentrations of NaCl and SDS, where Aβ(1−40) still required more than 8 h at 37 °C to form fibrils on the quartz. At low concentrations of NaCl (<0.3 M NaCl) or SDS (<0.3 mM SDS), we did not observe a large number of fibrils (Figure 2a,b). In contrast, at high concentrations of NaCl (0.5 or 1.0 M) and SDS concentrations at a level near CMC (0.3 or 0.5 mM), numerous amyloid fibrils were observed, producing spherical assemblies (Figure 2c−h). Densely packed spherical assemblies correspond to the spherulites reported previously by us (*27*) and others (*41*). The radial pattern of fibril growth suggests the formation of largely clustered seeds attached to the surface.

Interestingly, we often observed remarkably long fibrils protruding from the spherulitic cores (Figure 2e,f). It seems that the frequency with which long fibrils form is inversely correlated with the density of spherulitic cores, suggesting that the interactions of neighboring fibrils control the overall morphology. Fibrils of more than 150 μm demonstrate persistent growth under optimal conditions, consistent with a previous study of seed-dependent growth (*26*).

More interestingly, we observed a unique wormlike morphology (Figures 3c,d and 4), fundamentally distinct from the long and straight type fibrils (Figure 3a,b). The wormlike fibrils extended in an almost unlimited fashion (>500 μm), although we could not follow the trail exactly. Branching of the wormlike fibrils was also suggested from TIRFM images (Figures 3c,d and 4; see also Figure 7l−o). Careful inspection of TIRFM images indicated that the crossing points of overlapping fibrils are brighter in fluorescence than other regions (Figure 4). Accordingly, we can distinguish the apparent overlapping of fibrils from real branching of a single

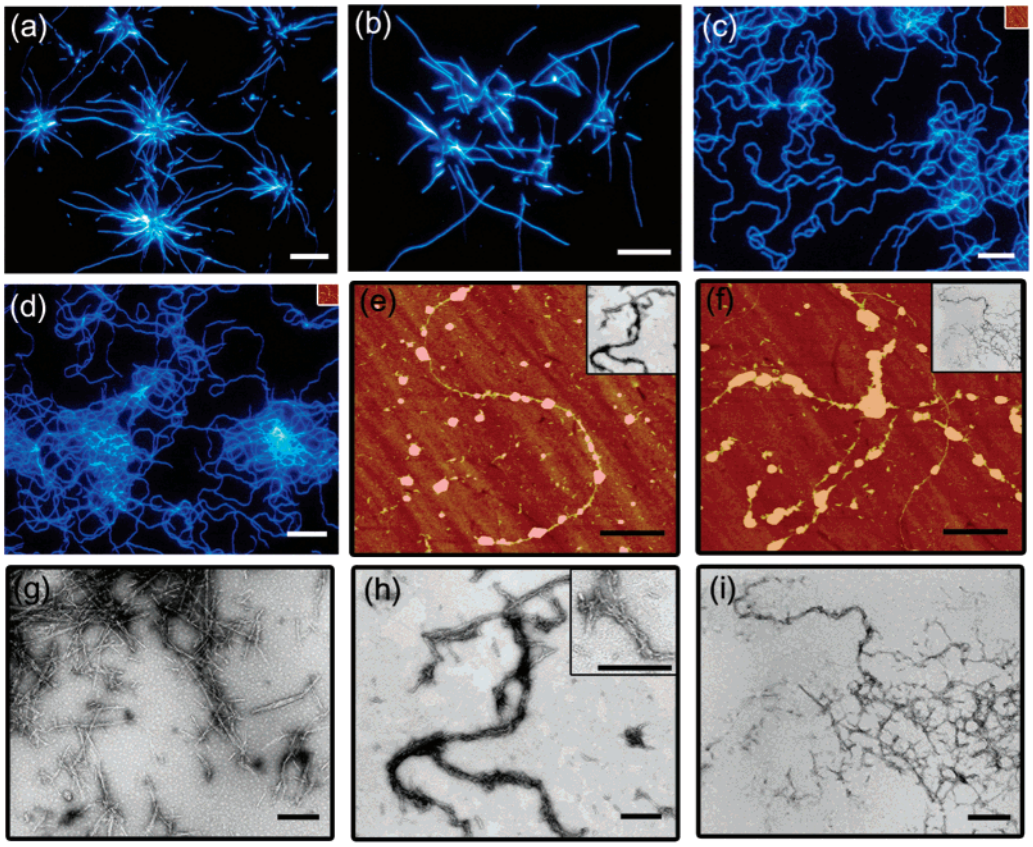

FIGURE 3: Variation in morphology of Aβ(1−40) fibrils and underlying protofibrillar assemblies. (a−d) TIRFM images showed straight fibrils (a and b) and wormlike fibrils (c and d) formed in 0.5 mM SDS and 0.5 M NaCl. (e and f) AFM images obtained by direct scanning of the quartz surface showing that the wormlike fibrils were made of many short fibrillar blocks. (g−i) TEM images of straight fibrils (g) and wormlike fibrils (h and i). The inset of panel h shows assemblies of short filaments with an expansion of 2-fold. To compare the scales of the TIRFM, AFM, and TEM images, AFM images (e and f) were inserted into TIRFM images (c and d) and TEM images (h and i) were inserted into AFM images (e and f). The scale bars represent 10 μm for TIRFM, 1 μm for AFM, and 200 nm for TEM.

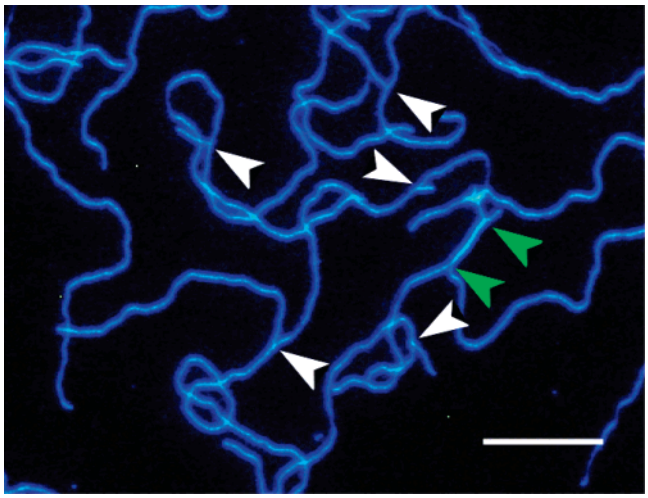

FIGURE 4: Random-walk-like growth of Aβ(1−40) wormlike fibrils with branching. The bottom left corner of Figure 3c was expanded. The white arrowheads indicate presumable branching points during growth. The green arrowheads indicate that the region between them brighter than other regions is made of two fibrils associated laterally.

fibril producing two equivalent daughter fibrils. For example, the region between two green arrowheads in Figure 4 is brighter than other regions, indicating that it is made of two fibrils. However, it remains unknown if this is caused by apparent overlapping of two independent fibrils or tight lateral association of two fibrils producing a thicker fibril.

The straight and wormlike fibrils were analyzed in detail using TEM and AFM. First, we examined by TEM the straight fibrils in spherulitic structures prepared on the quartz slide glass surface by transferring them to a carbon-coated copper grid (see Materials and Methods). In this method, it is likely that some fibrillar assemblies were partly broken during the transfer from the quartz surface to the carbon-coated copper grids. However, our TEM observation (Figure 3g) showed basically the same rigid fibrils that were observed by TIRFM (Figure 3a,b).

As for wormlike fibrils, TEM images revealed unexpected structures. Many blocks of short straight fibrils assembled laterally to form relatively thick and wavy fibrils (Figure 3h,i). Intriguingly, fibril blocks did not align in the same direction, probably because of the loose lateral packing, leading to a random-walk-like elongation (Figure 3h, inset). This pattern of association of short fibrils resembles the molecular alignment in a nematic liquid crystal. TEM images also suggested branching of wormlike fibrils. We also observed via AFM wormlike fibrils prepared on a quartz slide. The quartz surface was scanned directly by AFM (Figure 3e,f), revealing long and flexible fibrils consisting of many short fibrils. Considering the difference in the image scales, the wavy morphologies revealed by AFM and TEM reproduce smooth wormlike morphologies revealed by TIRFM. Although the TEM images of panels h and i of Figure 3 seem to have a slightly different character in their

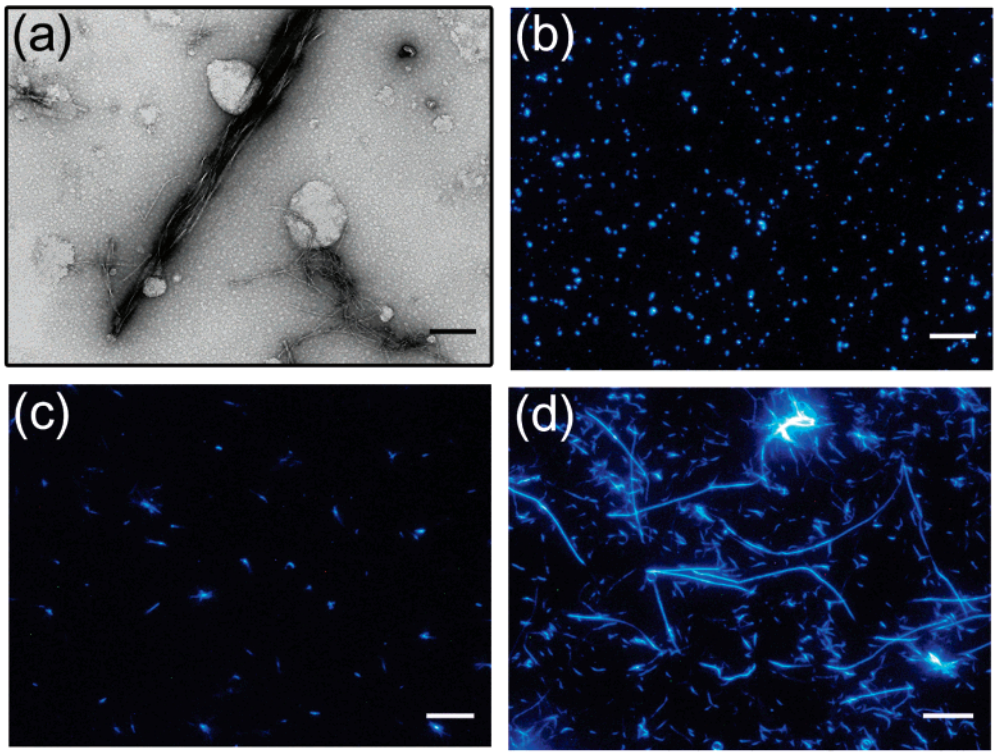

FIGURE 5: Seed-dependent growth of Aβ(1−40) fibrils at pH 7.5. The formation of Aβ(1−40) fibrils in the presence of 0.5 mM SDS and 0.5 M NaCl. (a) TEM image of Aβ(1−40) fibrils formed in a plastic tube. (b) TIRFM image of Aβ(1−40) seed fibrils after sonication. The many dots represent sonication-induced seed fibrils. (c and d) Seed-dependent growth of Aβ(1−40) fibrils at 0 (c) and 120 min (d). The image taken at 0 min shows many short fibrils. After 120 min, a large number of straight fibrils were observed. The scale bar represents 200 nm for TEM and 10 μm for TIRFM.

morphologies, this may represent the difficulty of transferring the fibrils prepared on the quartz slide glass surface to a carbon-coated copper grid for TEM. Taken together, the AFM, TEM, and TIRFM images were consistent, clarifying how the self-assembly of short and rigid blocks of Aβ(1−40) fibrils creates unique wormlike supramolecular assemblies.

In our TIRFM experiments at 0.5 or 1.0 M NaCl and 0.3 or 0.5 mM SDS, the spherulitic structures of Aβ(1−40) were major species and the wormlike fibrils were less often observed. Importantly, once the formation of fibrils was observed, the TIRFM images were independent of the locations on the quartz plate, revealing similar fibrillar images at many places on the quartz plate (Figure S1 for wormlike fibrils and Figure S2 for spherulitic structures). In other words, although there are distinct types of fibrillar morphologies, each quartz plate can produce only one of them. Statistically, among ~60 plates we prepared for fibril growth, the proportions of spherulitic structures, wormlike fibrils, and others, including failed samples, were 58, 27, and 15%, respectively. Although a subtle difference in the surface properties of quartz slides seems to be responsible for creating distinct supramolecular structures, the exact mechanism leading to distinct morphologies is unknown.

Seed-Dependent Growth of Aβ(1−40) Fibrils on the Quartz Surface. Because we observed unique fibrils of Aβ(1−40) without seeds on the quartz surface, we also examined the seed-dependent growth with the same slide glass under the same conditions (Figure 5). First, we prepared Aβ(1−40) fibrils in plastic tubes, which were used as seeds. The samples were incubated for 24 h, and the fibrils that formed were checked by TEM (Figure 5a). TEM images showed straight fibrils with a diameter of 11 ± 2 nm and various lengths. Then, the seed fibrils were sonicated and checked by TIRFM, revealing many dotlike fibrils (Figure 5b). When the seed samples were added to Aβ(1−40) monomers, the seeding reaction started immediately. Because the sample preparation required 5 min (i.e., dead time for TIRFM experiments), the image at 0 min already revealed many short fibrils (Figure 5c). After 120 min, many long and short fibrils were formed on the quartz surface (Figure 5d). These results confirmed that the morphology of straight fibrils is reproduced by the seed-dependent Aβ(1−40) fibril growth on the quartz surface, distinct from the spontaneous fibrillation.

Self-Assembly of Aβ(1−42) into Amyloid Fibrils on the Quartz Surface. We also investigated the spontaneous fibrillation of Aβ(1−42), another main component of senile amyloid plaques (Figure 6). Under the same conditions that were used for Aβ(1−40) (i.e., 0.5 M NaCl and 0.5 mM SDS without seeds), many aggregate-like structures were observed after incubation for 12 h (Figure 6a). Aβ(1−42) forms nuclei for spontaneous fibrillation much faster than Aβ(1−40). Additionally, SDS accelerates the fibrillation. Thus, in the presence of SDS, explosive fibrillation of Aβ(1−42) resulted in the formation of a large number of short fibrils, minimizing the effects of interactions with the surface. In the absence of SDS at 0.1 M NaCl, Aβ(1−42) formed long fibrils on the quartz surface, resembling the straight fibrils of Aβ(1−40) (Figure 6b). However, we observed neither wormlike fibrils nor spherulitic clusters of long fibrils, suggesting that Aβ(1−40) and Aβ(1−42) differ in how they interact with surfaces during the spontaneous formation of fibrils.

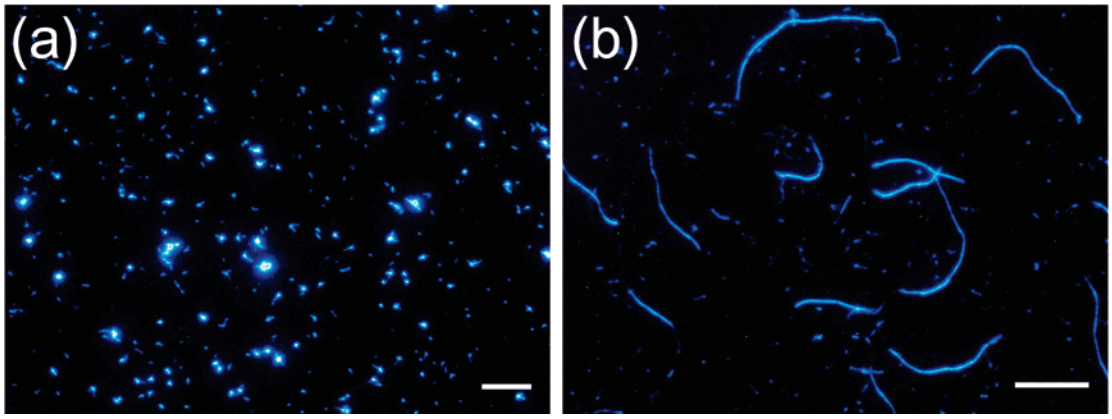

FIGURE 6: Formation of Aβ(1−42) fibrils without seeds at pH 7.5. Spontaneous fibrillation at 0.5 M NaCl with 0.5 mM SDS (a) and at 0.1 M NaCl without SDS (b) was examined by TIRFM. Many dotlike structures were formed in the presence of 0.5 mM SDS. Without SDS, long fibrils were detected. The scale bar represents 10 μm.

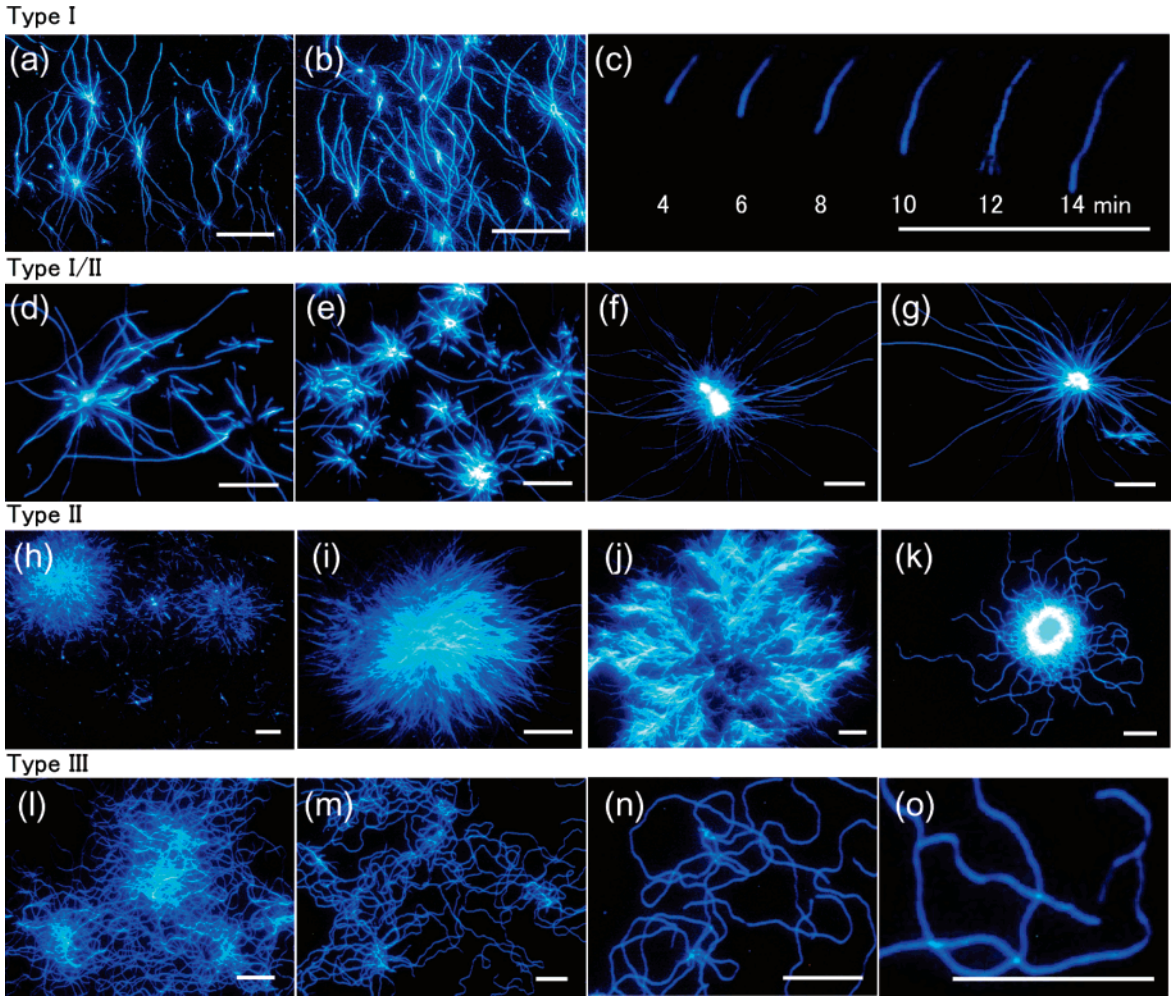

FIGURE 7: Gallery of Aβ(1−40) supramolecular fibrillar assemblies painted with ThT. (a−c) Type I straight and rigid fibrils taken from Ban et al. (*26*). Fibrils formed seed-dependently (a and b). The real-time observation of single fibril growth showing transient fraying at 12 min (c). (d−g) Mixed architecture of type I and II fibrils (type I/II) formed in 0.5 M NaCl and 0.5 mM SDS (d and e) or in 0.5 M NaCl and 0.3 mM SDS (f and g). (h−k) Type II spherulitic amyloid assemblies. Spherulitic structures made of type I fibrils on a PEI/PVS-coated quartz slide glass at 0.1 M NaCl taken from Ban et al. (*24*) (h). Spherulitic structures made of type I fibrils formed by spontaneous growth on the quartz slide glass at 0.5 M NaCl and 0.5 mM SDS (i) or at 1.0 M NaCl and 0.5 mM SDS (j). Spherulitic structures made of type III wormlike fibrils were also observed on the quartz slide glass at 0.5 M NaCl and 0.5 mM SDS (k). (l−o) Type III wormlike fibrils. The short fibrillar units associated laterally, leading to a random-walk-like fibril growth and branching. The scale bar represents 10 μm.

DISCUSSION

Classification of Amyloid Supermolecular Assemblies. In this study, to focus on the initial stages of fibrillation, we examined the spontaneous formation of Aβ(1−40) fibrils, for which a relatively high concentration of salt and a low concentration of SDS were added to accelerate the reaction. We observed various and remarkable images of Aβ(1−40) fibrils, suggesting that the effects of environmental factors,

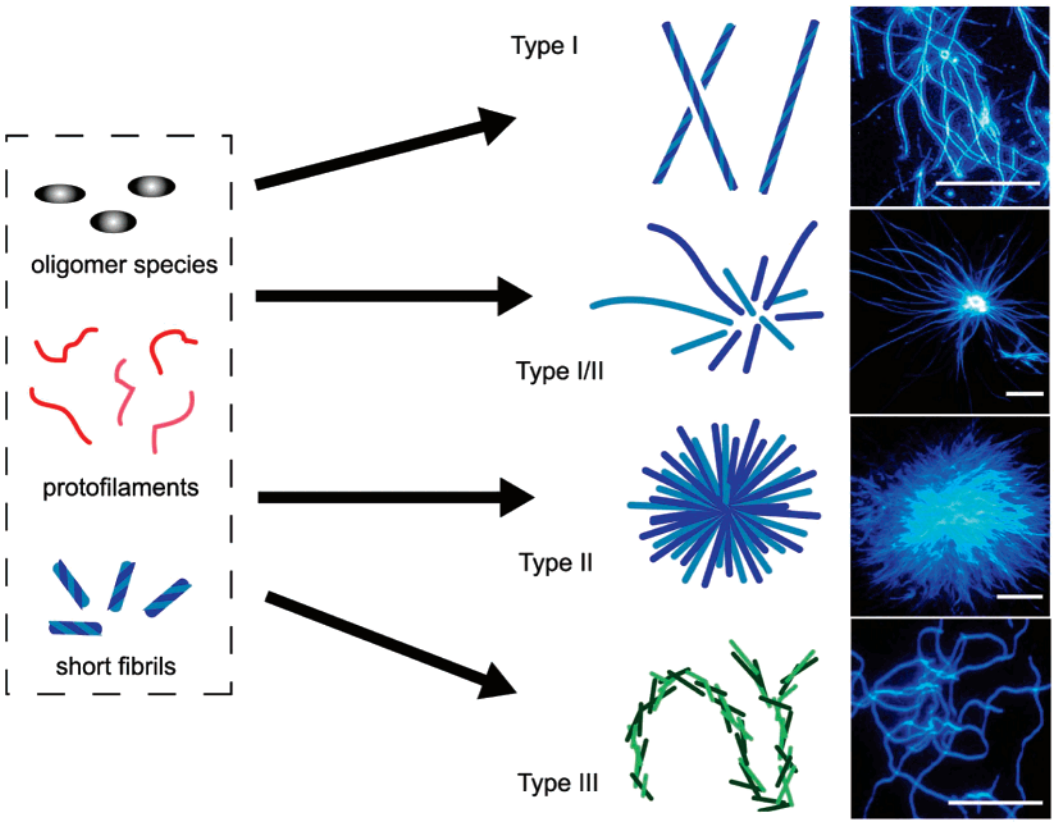

FIGURE 8: Schematic models of supramolecular fibrillar assemblies of Aβ(1−40) fibrils. Variation in morphology can arise at the level of oligomeric species, protofilaments, or initial short fibrils. They associate together on the quartz surface, creating three types of supramolecular fibrillar assemblies: straight fibrils (type I), spherulitic assemblies (type II), and wormlike fibrils (type III). A mixed architecture of type I and II fibrils (type I/II) was also observed when the internal density was coarse. It is noted that the different precursors are represented together in a box and that the relationships between amyloid precursors and final products remain unclear.

in particular, the interactions with the surface, were important in determining the morphology of fibrils. Under the conditions of TIRFM measurements, the reaction area was 18 mm $\times$ 18 mm and the distance between quartz slide and cover glass was 10 μm. Thus, it is possible that the narrow reaction space also plays an important role in creating the spherulitic amyloid assemblies, which we did not observe in test tubes. The importance of environmental factors is particularly true for the spontaneous fibrillation without seeding. The conformational states (oligomers, nucleus, or initial short fibrils) important for determining the subsequent morphology are probably unstable and easily influenced by a subtle change in environmental factors. In other words, the spontaneous formation of fibrils in contact with the surface disclosed multiple pathways leading to various forms of Aβ(1−40) fibrils.

On the basis of the various amyloid supramolecular fibrillar assemblies of Aβ(1−40) fibrils produced seed-dependently and -independently, there are three basic types of amyloid supramolecular fibrillar assemblies (Figures 7 and 8).

Type I fibrils are basic straight and rigid fibrils with a diameter of ~10−15 nm (Figure 7a−c). Although tremendous length can be achieved without lateral association, as observed for the seed-dependent growth on the quartz surface, the preparation in solution tends to form clustered fibrils. Precursors of mature amyloid fibrils can be oligomeric species, protofilaments, or initial short fibrils. Variation in morphology can arise at the level of these amyloid precursors. On the other hand, it is possible that different precursors as described above produce the similar mature fibrils. Thus, although it is clear that interactions with surfaces at the early stages affect the final morphological features, the relationships between amyloid precursors and final products remain unclear. This is also true for type II and III fibrils.

Type II fibrils are spherulitic amyloid assemblies typically made of type I basic fibrils. The wormlike fibrils (type III, see below) can also form spherulitic assemblies (Figure 7k). Spherulitic structures were observed in the spontaneous growth of Aβ(1−40) fibrils (Figure 2d,e,g,h and Figure 7h−k) as well as seed-dependent growth. The diameter reaches more than 30 μm. Probably, the clustered seeds or precursors initiate the fibril growth in a radial pattern. Internal density varies depending on the spherulitic assembly. Intriguingly, a densely packed spherulitic interior ensures concerted growth producing globular architectures. On the other hand, when the internal density is coarse, independent growth of constituent fibrils occurs, making a unique mixed architecture of type I and II fibrils, reminiscent of nerve synapses (Figure 2c,f and Figure 7d−g).

Another most intriguing morphology is the wormlike fibrils, type III (Figure 7l−o). Although the TIRFM images suggest flexible fibrils, the TEM and AFM images clarified that the wormlike fibrils are in fact made of rigid fibril blocks associated laterally (Figure 3e,f,h,i). Incomplete lateral association results in curvature of the longitudinal axis, producing the random-walk-like fibril growth. This incomplete lateral association may also produce branching of fibrils at the growing ends (Figure 4). Thus, in internal structure, the wormlike fibrils of Aβ(1−40) are distinct from the flexible

and thin protofilaments often observed for other amyloids (*42*, *43*). On the other hand, the remarkable length suggests that the nucleation of the wormlike fibrils does not occur frequently. As far as we know, an architecture as unique as that of type III fibrils has not been reported before.

In the case of Aβ(1−42), another main component of senile amyloid plaques in AD, we did not observe the variation in morphology that was observed for Aβ(1−40). Under these experimental conditions, fibrillation of Aβ(1−42) on the quartz occurred rapidly, producing a large number of dotlike structures. In accordance with this, recent studies have suggested a distinct molecular mechanism of fibrillation for the two peptides (*44*−*47*). Although the two peptides have different fibrillation properties, we expect the basic classification founded here to also apply to Aβ(1−42) fibrils. Moreover, spherulitic structures were also reported for a mouse model of AD (*33*), and in in vitro studies of insulin (*41*) and synthetic peptides (*48*). These results suggest that the amyloid fibrils have strong potential to form various high-order structures. We anticipate that this classification will apply to various amyloid fibrils.

Underlying Mechanism Responsible for the Variation in Morphology. However, it is still unclear what kind of species is responsible for the interaction with the quartz surface, leading to various assemblies. Variation in morphology can arise at the level of oligomeric species, protofilaments, or initial short fibrils. Various multiple-nucleation pathways have been reported: random nucleation of apomyoglobin (*49*), heterogeneous nucleation of insulin (*50*), and nucleation of Aβ monomer (*40*). Wogulis et al. (*34*) suggested a relationship between nucleation-dependent polymerization and neuronal cell death. The protofilaments may have several surfaces, allowing for packing in multiple ways (*22*). The Aβ(1−40) fibrils are formed by several protofilaments, the structure of which was reported by Petkova et al. (*51*, *52*). These results suggested that the Aβ protofilaments change their structure depending on the conditions, producing various supramolecular assemblies.

Finally, we address the effects of SDS and NaCl. In a previous study (*53*), upon examining the effects of fluorine-substituted alcohols (e.g., trifluoroethanol and hexafluoro-2-propanol) and SDS on the peptide fragments of β2m, we suggested that nonspecific aggregates of precursor proteins and hydrophobic cosolvents increase the chance of forming amyloid templates, thus promoting the fibrillation process. In the case of SDS, such aggregates accumulate maximally at ∼0.5 mM, a concentration slightly below the CMC. Under physiological conditions, hydrophobic cosolvents may be replaced by an amphiphilic environment like that on the basement membrane surface or by interaction with various amphiphilic compounds analogous to SDS. In particular, GM1 ganglioside bound to Aβ induced Aβ assembly in vivo (*39*). SDS may mimic the basement membrane environment, triggering the spontaneous formation of Aβ(1−40) fibrils under near-physiological conditions. Additionally, the formation of Aβ(1−40) fibrils was promoted in the presence of high concentrations of NaCl. In the presence of a high concentration of salt ions, salt bridges may play a more prominent role in the stabilization of the loop (Val 24−Lys 28) of Aβ(1−40) fibrils, thus forming nuclei rapidly (*40*).

CONCLUSIONS

We succeeded in visualizing the self-assembly of Aβ(1−40) into amyloid fibrils, obtaining various astonishing images. On the basis of unique images of fibrils, we classified the amyloid supramolecular fibrillar assemblies of Aβ(1−40) fibrils into three basic types: rigid and straight type I fibrils, spherulitic type II fibrils, and wormlike type III fibrils (Figures 7 and 8). Considering the increased morphological variability in the spontaneous fibrillation, interactions with surfaces at the early stages determine the final morphological features. Different amyloid supramolecular assemblies will have distinct biological impacts on the development and furthermore transmission of amyloidosis. Thus, clarifying the structural basis leading the various types of amyloid fibrils at the differed levels, from the structure of amyloid precursors to protofilament packing and interfibrillar interactions, is an important next step. The anatomy and taxonomy of amyloid supramolecular assemblies will be critical to progress in amyloid structural biology.

ACKNOWLEDGMENT

We thank Dr. Tetsuichi Wazawa (Tohoku University, Tohoku, Japan) for support with the TIRFM system. TEM images were recorded using a facility in the Research Center for Ultrahigh Voltage Electron Microscopy, Osaka University.

SUPPORTING INFORMATION AVAILABLE

A large number of Aβ(1−40) wormlike fibrils under the same quartz slide (Figure S1) and a large number of Aβ-(1−40) spherulitic structures under the same quartz slide (Figure S2). This material is available free of charge via the Internet at http://pubs.acs.org.

REFERENCES

1. Shastry, B. S. (2003) Neurodegenerative disorders of protein aggregation, *Neurochem. Int. 43*, 1−7.
2. Dobson, C. M. (2003) Protein folding and misfolding, *Nature 426*, 884−890.
3. Cohen, F. E., and Kelly, J. W. (2003) Therapeutic approaches to protein-misfolding diseases, *Nature 426*, 905−909.
4. Naiki, H., and Nakakuki, K. (1996) First-order kinetic model of Alzheimer's β-amyloid fibril extension in vitro, *Lab. Invest. 74*, 374−383.
5. Dobson, C. M. (2001) The structural basis of protein folding and its links with human disease, *Philos. Trans. R. Soc. London, Ser. B 356*, 133−145.
6. Zerovnik, E. (2002) Amyloid-fibril formation. Proposed mechanisms and relevance to conformational disease, *Eur. J. Biochem. 269*, 3362−3371.
7. McLaurin, J., Yang, D., Yip, C. M., and Fraser, P. E. (2000) Review: Modulating factors in amyloid-β fibril formation, *J. Struct. Biol. 130*, 259−270.
8. Fandrich, M., and Dobson, C. M. (2002) The behaviour of polyamino acids reveals an inverse side chain effect in amyloid structure formation, *EMBO J. 21*, 5682−5690.
9. Sasahara, K., Naiki, H., and Goto, Y. (2006) Exothermic effects observed upon heating of β_2-microglobulin monomers in the presence of amyloid seeds, *Biochemistry 45*, 8760−8769.
10. Wei, G., and Shea, J. E. (2006) Effects of solvent on the structure of the Alzheimer amyloid-β(25−35) peptide, *Biophys. J. 91*, 1638−1647.
11. Westermark, P., Benson, M. D., Buxbaum, J. N., Cohen, A. S., Frangione, B., Ikeda, S., Masters, C. L., Merlini, G., Saraiva, M. J., and Sipe, J. D. (2002) Amyloid fibril protein nomenclature−2002, *Amyloid 9*, 197−200.

12. Jin, L. W., Claborn, K. A., Kurimoto, M., Geday, M. A., Maezawa, I., Sohraby, F., Estrada, M., Kaminksy, W., and Kahr, B. (2003) Imaging linear birefringence and dichroism in cerebral amyloid pathologies, *Proc. Natl. Acad. Sci. U.S.A. 100*, 15294−15298.
13. Wetzel, R., Shivaprasad, S., and Williams, A. D. (2007) Plasticity of amyloid fibrils, *Biochemistry 46*, 1−10.
14. Kodali, R., and Wetzel, R. (2007) Polymorphism in the intermediates and products of amyloid assembly, *Curr. Opin. Struct. Biol. 17*, 48−57.
15. Tycko, R. (2004) Progress towards a molecular-level structural understanding of amyloid fibrils, *Curr. Opin. Struct. Biol. 14*, 96−103.
16. Tanaka, M., Chien, P., Naber, N., Cooke, R., and Weissman, J. S. (2004) Conformational variations in an infectious protein determine prion strain differences, *Nature 428*, 323−328.
17. Jones, E. M., and Surewicz, W. K. (2005) Fibril conformation as the basis of species- and strain-dependent seeding specificity of mammalian prion amyloids, *Cell 121*, 63−72.
18. Petkova, A. T., Leapman, R. D., Guo, Z., Yau, W. M., Mattson, M. P., and Tycko, R. (2005) Self-propagating, molecular-level polymorphism in Alzheimer's β-amyloid fibrils, *Science 307*, 262−265.
19. Luhrs, T., Ritter, C., Adrian, M., Riek-Loher, D., Bohrmann, B., Dobeli, H., Schubert, D., and Riek, R. (2005) 3D structure of Alzheimer's amyloid-β(1−42) fibrils, *Proc. Natl. Acad. Sci. U.S.A. 102*, 17342−17347.
20. Sunde, M., and Blake, C. (1997) The structure of amyloid fibrils by electron microscopy and X-ray diffraction, *Adv. Protein Chem. 50*, 123−159.
21. Jimenez, J. L., Nettleton, E. J., Bouchard, M., Robinson, C. V., Dobson, C. M., and Saibil, H. R. (2002) The protofilament structure of insulin amyloid fibrils, *Proc. Natl. Acad. Sci. U.S.A. 99*, 9196−9201.
22. Goldsbury, C. S., Wirtz, S., Muller, S. A., Sunderji, S., Wicki, P., Aebi, U., and Frey, P. (2000) Studies on the in vitro assembly of Aβ 1−40: Implications for the search for Aβ fibril formation inhibitors, *J. Struct. Biol. 130*, 217−231.
23. Ohhashi, Y., Kihara, M., Naiki, H., and Goto, Y. (2005) Ultrasonication-induced amyloid fibril formation of β_2-microglobulin, *J. Biol. Chem. 280*, 32843−32848.
24. Ban, T., Yamaguchi, K., and Goto, Y. (2006) Direct observation of amyloid fibril growth, propagation, and adaptation, *Acc. Chem. Res. 39*, 663−670.
25. Ban, T., Hamada, D., Hasegawa, K., Naiki, H., and Goto, Y. (2003) Direct observation of amyloid fibril growth monitored by thioflavin T fluorescence, *J. Biol. Chem. 278*, 16462−16465.
26. Ban, T., Hoshino, M., Takahashi, S., Hamada, D., Hasegawa, K., Naiki, H., and Goto, Y. (2004) Direct observation of Aβ amyloid fibril growth and inhibition, *J. Mol. Biol. 344*, 757−767.
27. Ban, T., Morigaki, K., Yagi, H., Kawasaki, T., Kobayashi, A., Yuba, S., Naiki, H., and Goto, Y. (2006) Real-time and single fibril observation of the formation of amyloid β spherulitic structures, *J. Biol. Chem. 281*, 33677−33683.
28. Selkoe, D. J. (1994) Alzheimer's disease: A central role for amyloid, *J. Neuropathol. Exp. Neurol. 53*, 438−447.
29. Serpell, L. C. (2000) Alzheimer's amyloid fibrils: Structure and assembly, *Biochim. Biophys. Acta 1502*, 16−30.
30. Hardy, J., and Selkoe, D. J. (2002) The amyloid hypothesis of Alzheimer's disease: Progress and problems on the road to therapeutics, *Science 297*, 353−356.
31. Gellermann, G. P., Appel, T. R., Tannert, A., Radestock, A., Hortschansky, P., Schroeckh, V., Leisner, C., Lutkepohl, T., Shtrasburg, S., Rocken, C., Pras, M., Linke, R. P., Diekmann, S., and Fandrich, M. (2005) Raft lipids as common components of human extracellular amyloid fibrils, *Proc. Natl. Acad. Sci. U.S.A. 102*, 6297−6302.
32. Gorbenko, G. P., and Kinnunen, P. K. (2006) The role of lipid-protein interactions in amyloid-type protein fibril formation, *Chem. Phys. Lipids 141*, 72−82.
33. Hsiao, K., Chapman, P., Nilsen, S., Eckman, C., Harigaya, Y., Younkin, S., Yang, F., and Cole, G. (1996) Correlative memory deficits, Aβ elevation, and amyloid plaques in transgenic mice, *Science 274*, 99−102.
34. Wogulis, M., Wright, S., Cunningham, D., Chilcote, T., Powell, K., and Rydel, R. E. (2005) Nucleation-dependent polymerization is an essential component of amyloid-mediated neuronal cell death, *J. Neurosci. 25*, 1071−1080.
35. Naiki, H., Higuchi, K., Hosokawa, M., and Takeda, T. (1989) Fluorometric determination of amyloid fibrils in vitro using the fluorescent dye, thioflavin T1, *Anal. Biochem. 177*, 244−249.
36. Wazawa, T., and Ueda, M. (2005) Total internal reflection fluorescence microscopy in single molecule nanobioscience, *Adv. Biochem. Eng. Biotechnol. 95*, 77−106.
37. Fraser, P. E., Nguyen, J. T., Chin, D. T., and Kirschner, D. A. (1992) Effects of sulfate ions on Alzheimer β/A4 peptide assemblies: Implications for amyloid fibril-proteoglycan interactions, *J. Neurochem. 59*, 1531−1540.
38. Yamamoto, S., Hasegawa, K., Yamaguchi, I., Tsutsumi, S., Kardos, J., Goto, Y., Gejyo, F., and Naiki, H. (2004) Low concentrations of sodium dodecyl sulfate induce the extension of β_2-microglobulin-related amyloid fibrils at a neutral pH, *Biochemistry 43*, 11075−11082.
39. Kakio, A., Nishimoto, S., Yanagisawa, K., Kozutsumi, Y., and Matsuzaki, K. (2002) Interactions of amyloid β-protein with various gangliosides in raft-like membranes: Importance of GM1 ganglioside-bound form as an endogenous seed for Alzheimer amyloid, *Biochemistry 41*, 7385−7390.
40. Cruz, L., Urbanc, B., Borreguero, J. M., Lazo, N. D., Teplow, D. B., and Stanley, H. E. (2005) Solvent and mutation effects on the nucleation of amyloid β-protein folding, *Proc. Natl. Acad. Sci. U.S.A. 102*, 18258−18263.
41. Krebs, M. R., Macphee, C. E., Miller, A. F., Dunlop, I. E., Dobson, C. M., and Donald, A. M. (2004) The formation of spherulites by amyloid fibrils of bovine insulin, *Proc. Natl. Acad. Sci. U.S.A. 101*, 14420−14424.
42. Hong, D. P., Gozu, M., Hasegawa, K., Naiki, H., and Goto, Y. (2002) Conformation of β_2-microglobulin amyloid fibrils analyzed by reduction of the disulfide bond, *J. Biol. Chem. 277*, 21554−21560.
43. McParland, V. J., Kad, N. M., Kalverda, A. P., Brown, A., Kirwin-Jones, P., Hunter, M. G., Sunde, M., and Radford, S. E. (2000) Partially unfolded states of β_2-microglobulin and amyloid formation in vitro, *Biochemistry 39*, 8735−8746.
44. Chen, Y. R., and Glabe, C. G. (2006) Distinct early folding and aggregation properties of Alzheimer amyloid-β peptides Aβ40 and Aβ42: Stable trimer or tetramer formation by Aβ42, *J. Biol. Chem. 281*, 24414−24422.
45. Deshpande, A., Mina, E., Glabe, C., and Busciglio, J. (2006) Different conformations of amyloid β induce neurotoxicity by distinct mechanisms in human cortical neurons, *J. Neurosci. 26*, 6011−6018.
46. Yan, Y., and Wang, C. (2006) Aβ42 is more rigid than Aβ40 at the C terminus: Implications for Aβ aggregation and toxicity, *J. Mol. Biol. 364*, 853−862.
47. Lim, K. H., Collver, H. H., Le, Y. T., Nagchowdhuri, P., and Kenney, J. M. (2007) Characterizations of distinct amyloidogenic conformations of the Aβ (1−40) and (1−42) peptides, *Biochem. Biophys. Res. Commun. 353*, 443−449.
48. Fezoui, Y., Hartley, D. M., Walsh, D. M., Selkoe, D. J., Osterhout, J. J., and Teplow, D. B. (2000) A de novo designed helix-turn-helix peptide forms nontoxic amyloid fibrils, *Nat. Struct. Biol. 7*, 1095−1099.
49. Fandrich, M., Zandomeneghi, G., Krebs, M. R., Kittler, M., Buder, K., Rossner, A., Heinemann, S. H., Dobson, C. M., and Diekmann, S. (2006) Apomyoglobin reveals a random-nucleation mechanism in amyloid protofibril formation, *Acta Histochem. 108*, 215−219.
50. Librizzi, F., and Rischel, C. (2005) The kinetic behavior of insulin fibrillation is determined by heterogeneous nucleation pathways, *Protein Sci. 14*, 3129−3134.
51. Petkova, A. T., Ishii, Y., Balbach, J. J., Antzutkin, O. N., Leapman, R. D., Delaglio, F., and Tycko, R. (2002) A structural model for Alzheimer's β-amyloid fibrils based on experimental constraints from solid state NMR, *Proc. Natl. Acad. Sci. U.S.A. 99*, 16742−16747.
52. Petkova, A. T., Yau, W. M., and Tycko, R. (2006) Experimental constraints on quaternary structure in Alzheimer's β-amyloid fibrils, *Biochemistry 45*, 498−512.
53. Yamaguchi, K., Naiki, H., and Goto, Y. (2006) Mechanism by which the amyloid-like fibrils of a β_2-microglobulin fragment are induced by fluorine-substituted alcohols, *J. Mol. Biol. 363*, 279−288.

BI701842N